SMARS: Sleep Monitoring via Ambient Radio Signals

Feng Zhang, *Student member, IEEE*[⋆†], Chenshu Wu, *Member, IEEE*[⋆†], Beibei Wang, *Senior member, IEEE*[⋆†], Min Wu, *Fellow, IEEE*[⋆†], Daniel Bugos[†], Hangfang Zhang[†], and K. J. Ray Liu, *Fellow, IEEE*[⋆†]

[⋆]*University of Maryland, College Park, MD 20742, USA.*
[†]*Origin Wireless, Inc., 7500 Greenway Center Drive, MD 20770, USA.*
[⋆]*Email: {fzhang15, cswu, bebewang, minwu, kjrliu}@umd.edu*
[†]*Email: {dan.bugos, hangfang.zhang}@originwireless.net*

Abstract—We present the model, design, and implementation of SMARS, the first practical Sleep Monitoring system that exploits Ambient Radio Signals to recognize sleep stages and assess sleep quality. This will enable a future smart home that monitors daily sleep in a ubiquitous, non-invasive and contactless manner, without instrumenting the subject's body or the bed. The key enabler underlying SMARS is a statistical model that accounts for all reflecting and scattering multipaths, allowing highly accurate and instantaneous breathing estimation with best-ever performance achieved on commodity devices. On this basis, SMARS then recognizes different sleep stages, including wake, rapid eye movement (REM), and non-REM (NREM), which was previously only possible with dedicated hardware. We implement a real-time system on commercial WiFi chipsets and deploy it in 6 homes, resulting in 32 nights of data in total. Our results demonstrate that SMARS yields a median absolute error of 0.47 breaths per minute (BPM) and a 95%-tile error of only 2.92 BPM for breathing estimation, and detects breathing robustly even when a person is 10 meters away from the link, or behind a wall. SMARS achieves a sleep staging accuracy of 88%, outperforming the prevalent unobtrusive commodity solutions using bed sensor or UWB radar. The performance is also validated upon a public sleep dataset of 20 patients. By achieving promising results with merely a single commodity RF link, we believe that SMARS will set the stage for a practical in-home sleep monitoring solution.

Index Terms—Breathing estimation, maximal ratio combining, radio signals, signal processing, sleep monitoring, vital signs monitoring, WiFi sensing.

1 Introduction

Sleep plays a vital role in an individual's health and well-being, both mentally and physically. It is well recognized that sleep quantity and quality is fundamentally related to health risks like cardiovascular disease, stroke, kidney failure, and diabetes, *etc*. Unfortunately, in a modern society, a number of people suffer from sleep disorders. As recently reported, 10% of the population suffers from chronic insomnia (which is even higher among elders) [1], and 1/3 of Americans do not get sufficient sleep [2]. Sleep monitoring emerges as an effective mechanism to manage the morbidity and mortality associated with sleep related disorders, in addition to providing insight on people's general wellbeing.

Over the past few decades, various sleep monitoring solutions have been proposed. Typically they measure sleep time, recognize different sleep stages, *i.e.*, wake, REM (Rapid Eye Movement) and NREM (Non-REM), and assess an individual's sleep quality. The medical gold standard is Polysomnography (PSG) using a number of contact sensors, which is usually expensive and cumbersome, limiting PSG to clinical usage for confirmed patients. Other approaches including photoplethysmography (PPG) and actigraphy (ACT) require users to wear dedicated sensors (*e.g.*, LED sensor and actimetry sensor) to measure vital signs (*e.g.*, respiratory rate and heart rate) and movements during sleep [3]. Ballistocardiogram (BCG) needs to instrument the mattress with an array of EMFi sensors to measure ballistic force. These approaches provide suitable solutions for those who need special care but are less-than-ideal for the public due to their cost and complexity. Recent efforts in mobile computing tackle in-home sleep monitoring using smartphones and wearables. These methods, however, only provide coarse-grained, less accurate measurements and fail to monitor vital signs like respiratory rate. In addition, mobiles and wearables are undesirable for elders and those with dementia.

Different from prevailing solutions, in this paper, we envision a future smart home that monitors daily sleep in a ubiquitous, non-invasive, contactless, and accurate manner, without instrumenting the body or the bed. We observe an opportunity towards such a system from two perspectives: 1) Clinical studies have shown that physiological activity varies between different sleep stages [4]. For example, breathing rate becomes irregular and rapid during REM sleep since brain oxygen consumption increases. During NREM sleep, breathing rate is slower and more stable, rendering the feasibility of sleep staging based on breathing monitoring. 2) Recent advances in wireless technology have demonstrated non-contact sensing of body motions in

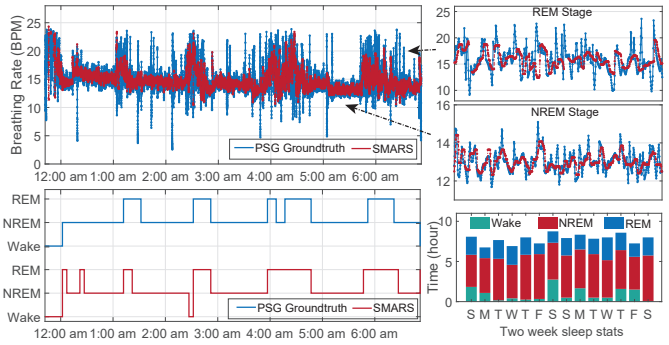

Fig. 1: An example of SMARS monitoring results

indoor environment [5], [6], [7], [8]. Chest and abdomen motions caused by breathing can alter radio signal propagations and thus modulate the received signals, from which it is then possible to decipher breathing. We explore a synergy between the two perspectives, resulting in a system that leverages ambient radio signals (*e.g.*, WiFi) to capture a person's breathing and motion during sleep and further monitor his/her sleep behaviors.

While early works have investigated the feasibility of RF-based breathing estimation and sleep monitoring, they either rely on specialized hardware like FMCW radar [6], [9], [10], or only work in controlled environments [5], [11], [12], [13]. Solutions based on dedicated radios are usually expensive and not ubiquitously applicable. Solutions using commodity devices typically require the user to lie still on a bed with radios exceedingly close to his/her chest. These solutions also fail in presence of extraneous motions or in Non-Line-Of-Sight (NLOS) scenarios. In addition, none of them can identify different sleep stages due to their limited accuracy in breathing estimation. Such limitations prevent them from becoming practical in-home sleep monitoring application.

In this paper, we present the model, design, and implementation of SMARS, the first practical Sleep Monitoring system that exploits commodity Ambient Radio Signals to recognize sleep stages and assess sleep quality. SMARS works in a non-obtrusive manner without any body contact. All that a user needs to do is to set up one single link between two commodity radios by, *e.g.*, simply placing a receiver in case a wireless router is already installed inside the home. SMARS advances the literature with a novel statistical model that allows highly accurate and instantaneous breathing estimation. On this basis, SMARS is able to distinguish different sleep stages (Fig. 1) via the tiny changes of the patterns of breathing rate over a period of time.

Specifically, SMARS excels in three unique aspects to deliver practical sleep monitoring. First of all, we devise a *statistical* model on motion in Channel State Information (CSI) that leverages all reflection and scattering multipaths indoors. Existing works usually assume a *geometrical* model with a few multipaths and one major path reflected off the human body (*e.g.*, using a 2-ray model developed for outdoor space) [7], [14], [15], [16]. Under real-world indoor environments, however, there could be as many as hundreds of multipaths [17], and signals not only reflect but also scatter off a person's body and other objects in the space. As a consequence, previous approaches fail in NLOS environments and cannot detect tiny, precise motions due to the lack of a dominant reflection path. In contrast, our model investigates the statistical characteristics of CSI without making such unrealistic assumptions, underlaying robust detection of arbitrary motions including breathing.

Second, SMARS achieves instantaneous, accurate and robust respiratory rate estimation. Most breathing estimation schemes [5], [11], [12], [14] assume constant breathing rate during a relatively large time window to gain sufficient frequency resolution. As a consequence, they lose fine-grained breathing variations during sleep. In addition, precise breathing motions can easily be buried in CSI measurement noises, rendering existing philosophies effective only in extraordinarily close proximity (typically within 2∼3 meters) without any extraneous motions. To improve time resolution, SMARS exploits the time-domain Auto-Correlation Function (ACF) to estimate breathing rate, which can report real-time breathing rates as frequent as every one second and make it possible to capture instantaneous breathing rate changes. By using ACF, SMARS also circumvents the use of noisy phase and the usually handcrafted CSI denoising procedure. More importantly, by eliminating the frequency offsets and thus synchronizing the CSI responses to breathing over different subcarriers, ACF allows us to perform Maximal Ratio Combining (MRC) to combine multiple subcarriers to maximize breathing signals in the optimal way. By doing so, we push the limit of the breathing signal to noise ratio (SNR) and thus significantly increase the sensing sensitivity for larger coverage as well as weaker breathing. Specifically, SMARS can reliably detect breathing when a person is 10 meters away from the link, or behind a wall, which is even better than specialized low-power radars [6], [9], [18].

Finally, based on the extracted breathing rates and motion statistics during sleep, we recognize different sleep stages (including wake, REM and NREM) and assess the overall sleep quantity and quality. Based on an in-depth understanding of the relationship between breathing rates and sleep stages, we extract distinctive breathing features for classification for sleep staging. To the best of our knowledge, none of existing works using commodity radios, *e.g.*, off-the-shelf WiFi, can achieve the same goal of staging sleep.

We have implemented a real-time system on commercial WiFi chipsets and evaluated its performance through extensive experiments. We deployed SMARS in 6 homes with 6 healthy subjects and collected 32 nights of data, and 5 out of 32 nights have PSG data. Our results demonstrate that SMARS yields a median absolute error of 0.47 BPM and a 95%-tile error of only 2.92 BPM for breathing estimation, and detects breathing robustly even when a person is 10 meters away from the link, or behind a wall. SMARS achieves sleep staging accuracy of 88%, outperforming the prevalent unobtrusive commodity solutions using bed sensor or UWB radar. The performance of breathing estimation is also validated upon a public sleep dataset of 20 patients. With these promising results, we believe SMARS can deliver meaningful sleep insights for clinical and regular use, taking an important step towards the actualization of a health monitoring smart home.

In a nutshell, our core contribution is SMARS, the first

system that enables a smart home to stage an inhabitant's sleep using commodity off-the-shelf WiFi devices, by achieving highly accurate and instantaneous breathing estimation in the wild. SMARS also contributes the first statistical model for understanding and capturing motions in CSI, which will promote various applications in wireless sensing.

The rest of the paper is organized as follows. We first review the literature in §2 and describe the design space in §3. We present SMARS design in §4, followed with the implementation and evaluation in §5. Then we conclude this paper in §6.

2 Related Works

SMARS is widely related to RF-based motion sensing, breathing estimation, and sleep monitoring, which have attracted numerous research interests. Most commercial solutions use contact sensors. For example, the medical gold standard PSG attaches a set of wired sensors to human body, which may cause significant discomfort and disrupt sleep and limits itself to clinical usage for patients. The research [4] shows that some of the vital signals, including respiratory rate, heart rate, are strongly correlated with sleep stages, and the work [19] shows the feasibility of sleep staging based on the breathing estimates alone. The technologies, such as PPG, ACT, and BCG [3], either require users to wear sensors or need to instrument the mattress to monitor the vital signs, making them suitable mainly for subjects who need special care. Similarly, novel in-ear sensor [20] is also less-than-ideal for the public. Some works leverage smartphone built-in sensors like accelerometers and microphones [21], [22], [23] to monitor movements and sound during sleep. Due to limited accuracy, these works only provide coarse-grained results and fail to stage sleep.

Non-contact solutions are more preferred and widely studied. Particularly, RF signals like WiFi, mmWave, UWB, and Doppler radar are recently investigated for breathing estimation and sleep monitoring [24], [25], [26], [27]. Many works exploit WiFi signals to estimate breathing [5], [13], [14], [18], [28], [29] and/or sleep monitoring [11], [12]. Despite that only controlled and short studied are conducted, these works cannot learn sleep stages due to large estimation errors. For example, the approaches proposed in [12] produce 95%-tile error of >10 BPM, as evaluated by [24]. FMCW radar [6], [9], [10] is also leveraged to monitor breathing. Among them, [9], [10] is capable of staging sleep, which, however, rely on specialized radios, rendering them not ubiquitously applicable. A number of works also aim at monitoring user motions and activities using RF signals, such as walking, standing, running, and various gestures, *e.g.*, [7], [30], [31], [32]. They mainly focus on large motions caused by activities when user is awake but cannot detect breathing during sleep. We envision our statistical model will stimulate a wide range of RF sensing applications that have been studied and that are yet to be imagined.

3 Goals and Scope

Different from controlled and short experiments conducted in previous studies, we envision that SMARS can be deployed in a smart home to monitor a person's overnight

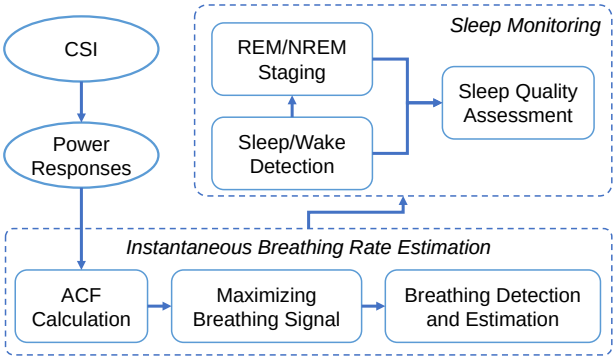

Fig. 2: Overview of SMARS Design

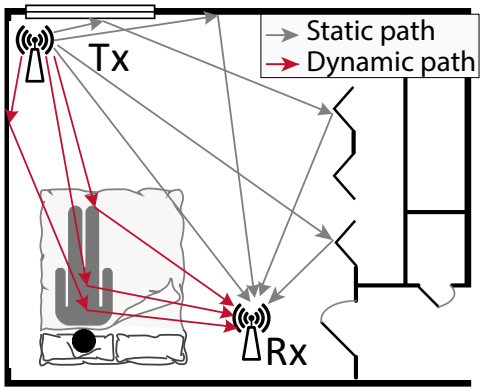

Fig. 3: Multipath propagation

breathing and movements in real-world scenarios, without body and bed instrumentation. SMARS can continuously track the subject's immediate respiratory rate changes during different sleep stages, precisely with sub-BPM accuracy and instantaneously with sub-second time resolution. Furthermore, the system, built upon a single RF link, can monitor breathing at distances up to 10 meters or behind a wall, providing a good coverage for common bedrooms. In addition, the breathing estimation is robust to various sleep positions and postures, and independent from different environments or subjects. Last, considering practical in-home use, SMARS is designed based on commodity off-the-shelf devices, especially those already existing in today's smart homes, *e.g.*, WiFi routers. The system works with fairly low sampling rate of 30 Hz or even 10 Hz, producing negligible impacts on in-home wireless connections.

SMARS also provides the capability to detect extraneous motions (walking or other body motions beyond breathing), which could dominate breathing motion and render it not detectable[1]. SMARS can detect arbitrary motions and use the quasi-static periods without large motions for breathing estimation. SMARS then stages a person's overnight sleep by fusing both motion statistics and breathing rates. SMARS is mainly designed for ubiquitous in-home sleep monitoring and not for critical sleep evaluation in hospitals and sleep labs.

1. Even wearables like chest bands cannot get reliable estimates under large non-breathing motions since breathing is buried in such cases.

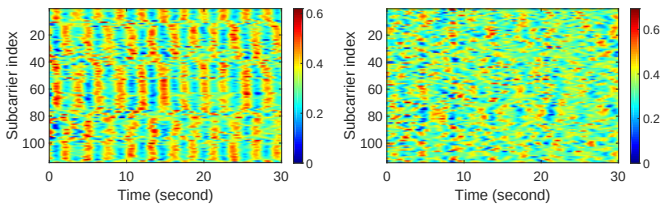

(a) LOS (b) NLOS

Fig. 4: The normalized CSI power response matrix with the presence of breathing signals. To facilitate the visualization, $G(t, f)$ is smoothed and normalized to the same amplitude over time for each subcarrier.

4 SMARS Design

In this section, we present the design of SMARS, which incorporates two key modules: 1) instantaneous breathing rate estimation; and 2) sleep monitoring as illustrated in Fig. 2.

4.1 Instantaneous Breathing Rate Estimation

In the following, we first introduce the concept of CSI and model the impact of human motion on the variations of CSI from a mathematical perspective. Then, we present a statistical approach to extract the breathing rate from the CSI data measured by a single subcarrier, and show how SMARS combines multiple subcarriers to maximize the SNR of breathing signals.

4.1.1 Theory of Operation

Given a wireless transmission pair each equipped with omnidirectional antennas, the Channel State Information (CSI), for the fading multipath channel at time t, is commonly modeled as [33]

$$H(t, f) = \sum_{l \in \Omega} a_l(t) \exp(-j2\pi f \tau_l(t)), \tag{1}$$

where $a_l(t)$ and $\tau_l(t)$ denote the complex amplitude and propagation delay of the l-th multipath component (MPC), respectively, and Ω denotes the set of MPCs. The propagation delay is a function of the propagation distance: $\tau_l(t) = \frac{d_l(t)}{c}$, where c is the speed of light and $d_l(t)$ is the traveled distance of the l-th MPC. f denotes the particular frequency where the channel is measured. For example, in an OFDM-based communication system, such as WiFi, LTE, 5G, *etc.*, the CSI is measured at each subcarrier with frequency f.

CSI depicts how radio signals propagate from a transmitter (Tx) to a receiver (Rx), *e.g.*, reflected or scattered off all reflectors in the space such as the walls, furniture, human bodies, *etc.*, and is highly sensitive to environmental perturbations. Any body motions, including tiny chest and abdomen movements during breathing [34], will alter the paths of signal propagation and thus modulate the wireless signal before it arrives at the receiver, allowing SMARS to capture these motions and monitor human's sleep from the measured CSI time series.

4.1.2 Modeling Motion in CSI

Most of the existing works adopt an overly simplified two-ray model [7], [15], which incorporates the direct path between the Tx and Rx and the reflection path that is reflected off the surface of human body, to analyze the effect of human motion on the CSI, and accordingly attempt to geometrically interpret multipath constructive and destructive interferences. However, the two-ray model are developed for and only hold in outdoor environments [16], which is not suitable for indoor environments. This is because, in reality, signals bouncing off human body may reflect, scatter, and diffract before finally being superimposed at the receiver, producing up to hundreds of multipaths indoors [17], as illustrated in Fig. 3. As a result, existing methods can only work in clear LOS scenarios with strong breathing in proximity, where a dominant reflection path exists. A more realistic model is demanded for practical motion and breathing sensing.

Consider the case when there is a static person breathing indoors with a cycle of T_b seconds. As shown in Fig. 3, the MPCs can be classified into two sets: Ω_s and $\Omega_d(t)$, where Ω_s denotes the set of time-invariant MPCs, *e.g.*, reflected off the floor and walls, and $\Omega_d(t)$ denotes the set of time-varying MPCs, *e.g.*, reflected off the human body. Due to the periodic chest or abdomen movement during normal breathing, the propagation distance $d_l(t)$ of each MPC $\forall l \in \Omega_d(t)$ changes periodically with the same cycle as the breathing movement, *i.e.*, $d_l(t + T_b) = d_l(t)$. Since the amplitude of breathing movement is small, the change in the propagation distance for each dynamic path is also small. Therefore, it is reasonable to assume that the complex amplitude of each MPC $a_l(t)$ is time-invariant within a sufficiently short period. Thus the CSI can be written as

$$\begin{aligned} H(t, f) &= \sum_{l_s \in \Omega_s} a_{l_s} \exp(-j2\pi f \frac{d_{l_s}}{c}) \\ &\quad + \sum_{l_d \in \Omega_d(t)} a_{l_d} \exp(-j2\pi f \frac{d_{l_d}(t)}{c}) \\ &\triangleq H_s(f) + H_d(t, f), \end{aligned} \tag{2}$$

where $H_s(f)$ and $H_d(t, f)$ denote the contribution of the time-invariant MPCs and time-varying MPCs, respectively.

In real measurements, $H(t, f)$ is corrupted by the phase noise, caused by the timing and frequency synchronization offsets, and the additive thermal noise $\epsilon(t, f)$, and the reported CSI $\tilde{H}(t, f)$ can be expressed as

$$\tilde{H}(t, f) = \exp(-j(\alpha(t) + \beta(t)f))H(t, f) + \epsilon(t, f), \tag{3}$$

where $\alpha(t)$ and $\beta(t)$ are the random initial and linear phase distortions at time t, respectively. Define the *channel power response* $G(t, f)$ as the square of the magnitude of $\tilde{H}(t, f)$:

$$\begin{aligned} G(t, f) &\triangleq |\tilde{H}(t, f)|^2 \\ &= |H(t, f)|^2 + 2\mathrm{Re}\{n^*(t, f)H(t, f) \\ &\quad \exp(-j(\alpha(t) + \beta(t)f))\} + |\epsilon(t, f)|^2 \\ &\triangleq |H(t, f)|^2 + \varepsilon(t, f), \end{aligned} \tag{4}$$

where the superscript * denotes the operator of complex conjugate, the operator $\mathrm{Re}\{x\}$ denotes the real part of x, and $\varepsilon(t, f)$ is defined as the noise term, which can be

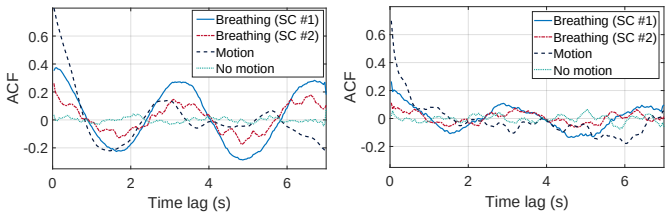

(a) LOS (b) NLOS

Fig. 5: The illustrations of ACFs under LOS and NLOS scenarios.

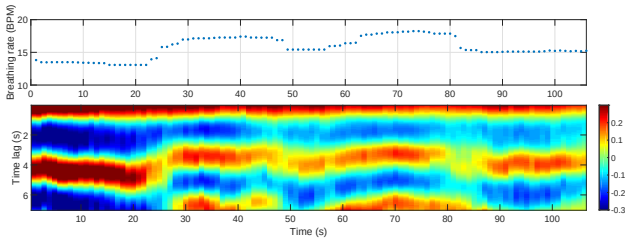

Fig. 6: Breathing rate estimation from ACFs.

approximated as additive white Gaussian noise (AWGN) with variance $\sigma^2(f)$ and is statistically independent of $H(t,f)$ [35]. From (2) and the fact that $d_l(t+T_b) = d_l(t)$, $\forall l \in \Omega_d(t)$, we have $|H(t+T_b,f)|^2 = |H(t,f)|^2$. Thus $G(t,f)$ is modeled as a noisy periodic signal with a period of T_b.

As shown in Fig. 4, we measure the CSI power response $G(t,f)$ using a pair of commercial WiFi devices for both the two cases, when a subject is breathing in a LOS and a NLOS location with respect to the transmission pair, respectively. For the LOS case, the strength of the measured breathing signal is strong and the periodic pattern can be easily observed by most subcarriers as shown in Fig. 4(a). For the NLOS case as shown in Fig. 4(b), however, there are no apparent periodic patterns that can be observed since the breathing signal is much weaker.

Note that $G(t,f)$ is a result of numerous multipath components [17] adding up together in a complex way expressed in (2). As shown in Fig. 4(a), both the amplitudes and the phases of the breathing signal measured by CSI are different for different subcarriers. Accordingly, it is reasonable to express $|H(t,f)|^2$ in the following form:

$$|H(t,f)|^2 = g(f)b(t-\Delta t_f), \tag{5}$$

where $b(t)$ denotes a periodic stationary breathing signal with zero mean, which is related to the movement of the chest and abdomen, and $g(f)$ and Δt_f stand for the gain and the random initial phase of the breathing signal measured at the frequency f, respectively.

Combining (4) and (5), the received signal at subcarrier with frequency f is expressed as

$$G(t,f) = g(f)b(t-\Delta t_f) + \varepsilon(t,f). \tag{6}$$

Breathing estimation is then conducted based on the power response $G(t,f)$, which circumvents the use of noisy CSI phase and the usually handcrafted phase cleaning step.

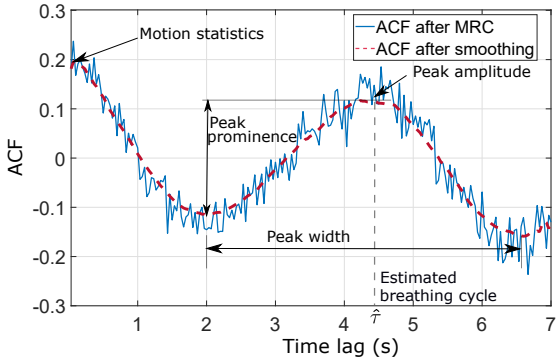

Fig. 7: Features extracted from the derived ACF for breathing detection and estimation.

4.1.3 Estimating Breathing Rate

Observing that breathing signal is periodic, previous methods usually perform frequency analysis on the CSI data collected in a time window to estimate breathing rate [5], [11], [12]. These methods require a large delay (*e.g.*, more than 30 seconds) to gain better frequency resolution, and cannot observe immediate breathing rate changes, since breathing rate is assumed to be constant during the time window. Differently in SMARS, we adopt a statistical approach by examining the autocorrelation function (ACF) of CSI power response $G(t,f)$, which significantly shortens the time delay and produces instantaneous estimation.

ACF Calculation. The ACF for a stationary signal $x(t)$ is defined as follows:

$$\rho(\tau) = \frac{\mathrm{cov}[x(t), x(t+\tau)]}{\mathrm{cov}[x(t), x(t)]}, \tag{7}$$

where τ denotes the time lag, and $\mathrm{cov}[\cdot]$ denotes the covariance operator. Thus the ACF of $G(t,f)$ is computed as

$$\rho_G(\tau,f) = \frac{g^2(f)}{g^2(f)+\sigma^2(f)}\rho_b(\tau) + \frac{\sigma^2(f)}{g^2(f)+\sigma^2(f)}\delta(\tau), \tag{8}$$

where $\rho_b(\tau)$ is the ACF of $b(t)$, and $\delta(\tau)$ denotes the Dirichlet function. Define $k(f) \triangleq \frac{g^2(f)}{g^2(f)+\sigma^2(f)}$ as the normalized channel gain, and for $\tau \neq 0$, we have

$$\rho_G(\tau,f) = k(f)\rho_b(\tau). \tag{9}$$

In practice, the sample ACF is used instead [36], which is an estimate of the ACF, and we use $n(\tau,f)$ to stand for the estimation noise of the ACF, *i.e.*,

$$\hat{\rho}_G(\tau,f) = k(f)\rho_b(\tau) + n(\tau,f). \tag{10}$$

As shown in Fig. 5, when there is a breathing signal, the ACF will exhibit a definite peak at a certain delay (although the peak value may differ over different subcarriers), contributed by the periodic breathing motions. On the contrary, no prominent peaks can be observed on any subcarrier when there is no breathing (*i.e.*, no periodic motions). In principle, as shown in Fig. 6, a time delay slightly longer than one breathing cycle (*e.g.*, 5 to 7 seconds) is sufficient to pick up the first breathing rate and later on instantaneous estimates can be produced every one second.

Motion Statistic. Prior to breathing estimation, a key step is to examine whether there exists any extra large

motions. As mentioned previously, breathing will easily be buried in other large body motions, and should not be estimated in such case. As shown in Fig. 5(a) and (b), the first time lag of the ACF of a subcarrier, named as the *motion statistic* in the following, indicates the strength of total motions, including periodic and non-periodic motions, existing in the monitored area. A very large motion statistic indicates the presence of large motions, such as walking and standing up, and a very small motion statistic that is close to 0 indicates that there is no significant motion in the environment. When there is only breathing motion in the monitored area, the motion statistic of each subcarrier shows the sensitivity of that subcarrier to the breathing motion.

Breathing Detection and Estimation. Based on the calculated ACF, SMARS first detects the presence/absence of breathing and, if present, it then estimates the breathing rate. As shown in Fig. 7, for a subcarrier with frequency f, we extract the following five features from $\hat{\rho}_G(\tau, f)$ after the locally estimated scatterplot smoothing (LOESS) for breathing detection [37], in addition to the *motion statistic*:

1) *Peak prominence*: the vertical distance between a peak value and the largest height of the adjacent valleys, which measures the likelihood of the existence of the peak;
2) *Peak width*: the horizontal distance between the two adjacent valleys, which also measures the likelihood of the existence of a peak;
3) *Peak amplitude*: the height of a peak, which measures the amplitude of the ACF of the breathing signal and will be comparable to the value of motion statistic in presence of only breathing motion;
4) *Motion interference ratio*: the ratio between the motion statistic and peak amplitude, which measures the degree of the interference of the non-breathing motion, such as body movements, walking, standing up, typing keyboard, *etc.*, in the environment;
5) *Peak location*: the horizontal distance between the origin and the peak (*i.e.*, time lags), which measures the breathing cycle.

In general, the larger the motion statistic, peak prominence, peak width, peak amplitude and the smaller the motion interference ratio, the more likely is the presence of the breathing signal. In other words, a breathing signal is detected only if the motion statistic, peak prominence, peak width and peak amplitude are all larger than their respective preset thresholds and the motion interference ratio is smaller than its preset threshold. Then, once there is a breathing signal, the breathing rate can be estimated as $\mathrm{BR} = 60/\hat{\tau}$ BPM, where $\hat{\tau}$ is the location (*i.e.*, time lags) of the first dominant peak of $\hat{\rho}_G(\tau, f)$. Note that SMARS prioritizes all the potential local peaks of $\hat{\rho}_G(\tau, f)$ based on their locations, and the peak with a smaller time lag value has a higher priority.

4.1.4 Maximizing Breathing Signal

In practice, the SNR of the breathing signal on each subcarrier modulated by minute breathing motions is very low, especially when the person being monitored is far away from the link, covered by quilts, or behind the wall. As shown in Fig. 5, the SNR of the ACF for NLOS breathing

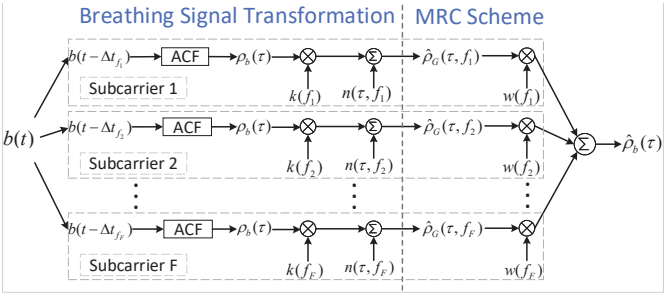

Fig. 8: The diagram of MRC on ACF of breathing signal.

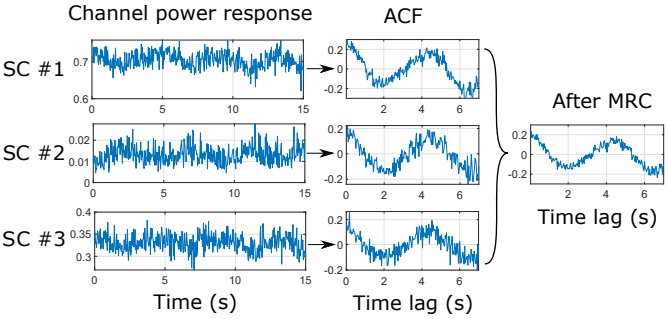

Fig. 9: Example of MRC scheme for breathing signal maximization. Subcarrier (SC) 1, 2 and 3 rank the first, sixth and tenth respectively among the 114 subcarriers from a link according to $\hat{k}(f)$.

is significantly lower than that for LOS scenarios. Previous approaches attempt to select a set of best subcarriers among others, or take an ensemble average over all subcarriers to improve the quality of the breathing signal strength [5], [11], [12], [13]. However, we make the following observations that demonstrate the flaws of these methods: 1) Any single subcarrier does not produce the optimal estimation, no matter what criteria is used for selection. 2) CSI amplitude or its variance is not an effective metric for subcarrier selection. The subcarrier with largest amplitude or variance usually does not capture the breathing signal to the best. 3) Due to frequency offsets across different subcarriers, CSI amplitudes responding to the person's breathing are unsynchronized and contain uncertain offsets (Fig. 4). Hence the CSI on different subcarriers cannot be directly averaged, which does not necessarily amplify, yet may instead rule out breathing signals. As a consequence, previous approaches do not produce reliable, not to mention optimal estimation.

To boost the breathing SNR, SMARS devises a novel scheme to combine the breathing signals measured on multiple subcarriers in an *optimal* manner. Our design is based on Maximal Ratio Combining (MRC), a general diversity fusion strategy with successful applications in wireless communications, that maximizes SNR by combining multiple received signals [38].

MRC Model. We first review the basic concept of MRC in telecommunications in the following. Let vector $\mathbf{x} = [x_1, \ldots, x_N]^T$ denote the received signal at N antennas, which can be written as $\mathbf{x} = \mathbf{h}u + \mathbf{n}$, where $\mathbf{h} = [h_1, \ldots, h_N]^T$ denotes the constant channel gains, u denotes the transmitted random signal with unit power, and $\mathbf{n} = [n_1, \ldots, n_N]^T$ stands for the identically and independently distributed (I.I.D.) additive white Gaussian

noise (AWGN) with variance σ^2. Let r denote the linearly combined signal:

$$r = \mathbf{w}^T\mathbf{x} = \mathbf{w}^T\mathbf{h}u + \mathbf{w}^T\mathbf{n}, \tag{11}$$

where $\mathbf{w} = [w_1, \ldots, w_N]^T$ denotes the normalized weight of each received signal at each antenna, that is, $\|\mathbf{w}\| = 1$. The SNR, denoted as γ, of the output signal r can be denoted as

$$\gamma = \frac{\mathbb{E}[|\mathbf{w}^T\mathbf{h}u|^2]}{\mathbb{E}[|\mathbf{w}^T\mathbf{n}|^2]} = \frac{|\mathbf{w}^T\mathbf{h}|^2}{\sigma^2}. \tag{12}$$

By the Cauchy-Schwarz inequality, we have $|\mathbf{w}^T\mathbf{h}|^2 \leq \|\mathbf{w}\|\|\mathbf{h}\|$. The equality is achieved when $\mathbf{w}$ is linearly proportional to $\mathbf{h}$, *i.e.*, $\mathbf{w}^* = \mathbf{h}/\|\mathbf{h}\|$, and the maximum of output SNR can be obtained as the sum of the SNR of received signals at each antenna, *i.e.*, $\gamma = \gamma_1 + \cdots + \gamma_N$, where $\gamma_i = |h_i|^2/\sigma^2$.

MRC on Breathing Signal. In the context of breathing estimation with CSI, the breathing signal $b(t)$ is measured by multiple subcarriers. The SNR of the breathing signal, denoted as $\gamma(f)$, measured on subcarrier with frequency f at time t is defined as

$$\begin{aligned}\gamma(f) &= \frac{\mathbb{E}[(g(f)b(t-\Delta t_f))^2]}{\mathbb{E}[\varepsilon^2(t,f)]} \\ &= \frac{g^2(f)\mathbb{E}(b^2(t-\Delta t_f))}{\sigma^2(f)},\end{aligned} \tag{13}$$

where $\mathbb{E}[\cdot]$ stands for the expectation operator. For convenience, the average power of the breathing signal $b(t)$ is normalized to unit power by definition, that is, $\mathbb{E}[b^2(t)] = 1$. Thus we have $\gamma(f) = g^2(f)/\sigma^2(f)$.

When applying MRC to exploit subcarrier diversity to maximize the overall SNR of the measured breathing signal optimally, however, we face three fundamental challenges:

1) The variance of the noise term in (6) is $\sigma^2(f)$, which is unknown and dependent on the frequency f, while MRC assumes the same variance of the noise for all the receiving elements;
2) The offset of the breathing signal Δt_f in (6) is incoherent for different subcarriers, while MRC requires that the transmitted signal is the same for all receiving elements;
3) The channel gain $g(f)$ in (6) is unknown, while MRC relies on the channel gain to compute the optimal combining weights for the receiving elements.

Fortunately, by using ACF instead of $G(t, f)$, SMARS successfully transforms the breathing signal into an appropriate form to apply MRC for optimal subcarrier combining.

Recall §4.1.3, when the breathing signal is extremely weak, *i.e.*, $k(f)$ is close to zero, $G(t, f)$ is dominated by the white noise and thus, each tap of its ACF follows a zero-mean normal distribution with equal variance $1/N$ [36], *i.e.*, $n(\tau, f) \sim \mathcal{N}(0, 1/N)$, where N is the number of samples used in the ACF estimation. Thus the variance of $n(\tau, f)$ is identical for different subcarriers, solving the first challenge.

As shown in Fig. 9, the ACF $\rho_b(\tau)$ are inherently synchronized over all subcarriers and is independent of the time origin. In other words, different subcarriers experience the same signal $\rho_b(\tau)$, which addresses the second challenge.

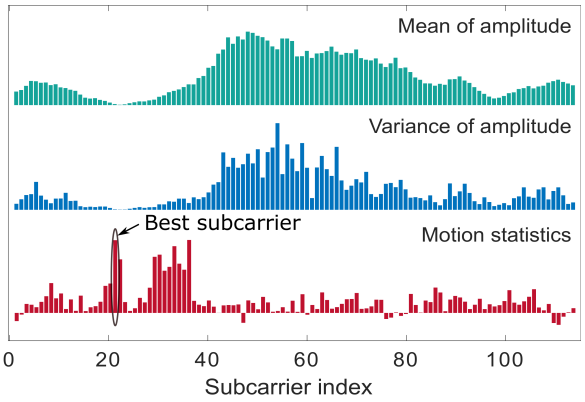

Fig. 10: Comparison of the subcarrier selection schemes. The best subcarriers selected by the mean and variance are merely ranked 113-th and 95-th, respectively, when considering their motion statistics.

Regarding the third challenge, the channel gain $k(f)$ can be estimated as follows. For the case of single subject breathing, recall (9), when $\tau \to 0$, we have

$$\lim_{\tau\to 0}\rho_G(\tau, f) = k(f)\lim_{\tau\to 0}\rho_b(\tau). \tag{14}$$

Since the movement of chest and abdomen is continuous, the breathing signal $b(t)$ is also continuous in time and we have $\lim_{\tau\to 0}\rho_b(\tau) = 1$, which leads to $\lim_{\tau\to 0}\rho_G(\tau, f) = k(f)$. As a result, when the channel sampling rate F_s is high enough, the quantity $\hat{\rho}_G(\tau = 1/F_s, f)$ is close to the channel gain $k(f)$. That is, $k(f)$ can be estimated as

$$\hat{k}(f) = \hat{\rho}_G(\tau = 1/F_s, f), \tag{15}$$

which is the same as the *motion statistic*. This is a key feature that underpins the use of MRC; otherwise one can still combine different subcarriers, but not optimally. To conclude, MRC can now be applied to the ACF of the breathing signal to maximize the SNR.

Maximizing Breathing SNR. We now maximize the SNR of the ACF of the breathing signal, instead of the SNR of the breathing signal, as in (5), which cannot be directly maximized since the channel gain and noise cannot be measured in CSI.

Recall (10) and that the variance of the noise term is approximated as $1/N$, and thus, the SNR of the ACF of each subcarrier can be estimated as $N\hat{k}^2(f)$. Since the SNR of the breathing signal after MRC is the additive of the SNR measured by each subcarrier, the SNR of the combined ACF is expressed as

$$\gamma = N\sum_{f\in\mathcal{F}}\hat{k}^2(f). \tag{16}$$

Given a fixed number of subcarriers and sample number of N, it will be maximized by setting the optimal weight $w^\star(f)$ to $\hat{\rho}_G(\tau = 1/F_s, f)$ in the following linear combination: $\forall\tau$,

$$\begin{aligned}\hat{\rho}_b(\tau) &= \sum_{f\in\mathcal{F}} w^\star(f)\hat{\rho}_G(\tau, f) \\ &= \sum_{f\in\mathcal{F}}\hat{\rho}_G(\tau = 1/F_s, f)\hat{\rho}_G(\tau, f).\end{aligned} \tag{17}$$

Here $\hat{\rho}_b(\tau)$ is the ACF of the combined signal.

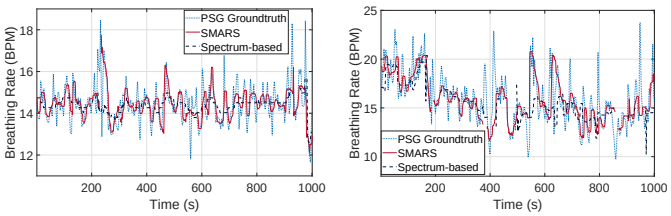

(a) NREM stage. (b) REM stage.

Fig. 11: Comparison between SMARS and spectrum-based method.

Fig. 8 summarizes the proposed scheme for breathing signal extraction and maximization. The left part of the figure shows the decomposition of the measured ACF of the channel power response when a person breathes normally in the monitored area, and the right part shows the MRC scheme for boosting the SNR of the ACF of the breathing signal. Fig. 9 depicts an illustrative example based on real-world measurements, where the SNR of the breathing signal is amplified by 2.5 dB compared to that obtained by the subcarrier with the largest variance and by 3.7 dB compared to that obtained by directly averaging all subcarriers. Fig. 10 further demonstrates the gains of our ACF-based MRC scheme and confirms our observations in §4.1.4 that amplitudes and their variances are not effective metrics for subcarrier selection. As seen, the subcarrier that is the most sensitive to motion (*i.e.*, holding the largest motion statistic) could experience very small amplitude and low variance.

Given the combined breathing signal with maximized SNR, SMARS then performs breathing detection and estimation, as described in §4.1.3, based on $\hat{\rho}_b(\tau)$, the combined ACF, instead of $\hat{\rho}_G(\tau, f)$ on a specific subcarrier, as illustrated in Fig. 6. The detailed procedures of the proposed breathing estimator have been summarized in Algorithm 1.

Algorithm 1 SMARS Breathing Estimation

Input: N consecutive CSI measurements till time t: $H(s, f)$, $s = t - \frac{N-1}{F_s}, ..., t - \frac{1}{F_s}, t$, and $f \in \mathcal{F}$;
Output: Breathing rate: BR(t), and motion statistic: MS(t).
1: Calculate the CSI power response: $G(s, f) \leftarrow |H(s, f)|^2$, for $\forall s$ and $\forall f$;
2: Calculate the ACF of each subcarrier f: $\hat{\rho}_G(\tau, f) \leftarrow \frac{1}{N} \sum_{s=t-\frac{N-1}{F_s}+\tau}^{t} \left(G(s-\tau, f) - \bar{G}(f)\right)\left(G(s, f) - \bar{G}(f)\right)$, where $\bar{G}(f)$ is the sample mean of the current window;
3: Aggregate ACF across all the subcarriers: $\hat{\rho}_b(\tau) = \sum_{f \in \mathcal{F}} \hat{\rho}_G(\tau = 1/F_s, f)\hat{\rho}_G(\tau, f)$;
4: Extract the six features related to the breathing signal from $\hat{\rho}_b(\tau)$ as described in §4.1.3;
5: BR$(t) \leftarrow 60/\hat{\tau}$ BPM, when breathing signal is detected, otherwise BR$(t) \leftarrow 0$, and MS$(t) \leftarrow \hat{\rho}_b(\tau = 1/F_s)$.

Remark. Traditional spectrum-based methods usually need a long duration of CSI measurements, *e.g.*, $T_w = 63$ seconds [39], where T_w denotes the duration of the window, to estimate the breathing frequency with an acceptable accuracy. By contrast, thanks to the proposed SNR boosting scheme, SMARS only needs a very short duration of CSI measurements, just slightly longer than one cycle of a breath as shown in Fig. 7, to harvest the tiny energy of breathing signal on multiple subcarriers, which enables SMARS to track time-varying breathing rates. In addition, since the breathing cycle is estimated in time domain, SMARS can achieve a much higher resolution and accuracy in breathing cycle estimation, $1/F_s$ seconds per breathing cycle, where F_s denotes the sampling rate of CSI measurements. For the above reasons, SMARS is able to track instantaneous changes of breathing rate with a high accuracy, as shown in Fig. 11, which provides much more detailed information about sleep stages.

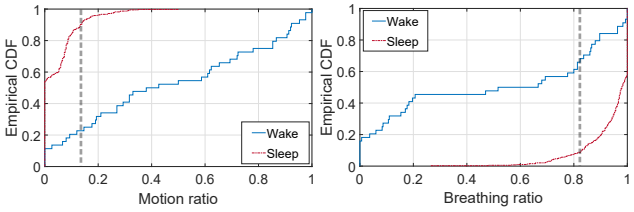

Fig. 12: Empirical CDFs for the motion ratio and breathing ratio under two states: wake and sleep.

4.2 Sleep Monitoring

In the following, the algorithm of sleep stage recognition of SMARS and sleep quality assessment are presented in §4.2.1 and §4.2.2, respectively.

4.2.1 Sleep Stage Recognition

SMARS divides the continuous motion and breathing estimates of overnight sleep into 300-second epochs[2]. For each epoch, SMARS recognizes three different sleep stages, *i.e.*, wake, REM sleep and NREM sleep[3]. The staging is performed in two steps: first, SMARS differentiates wake from sleep mainly by body motions; second, REM and NREM stages are further identified during sleep period.

Sleep/Wake Detection. The key insight to identify the sleep and wake states is that, more frequent body movements will be observed when a subject is awake, while mainly breathing motion presents when she/he is asleep. SMARS utilizes the motion statistic defined in §4.1 to distinguish between the two states, since bodily movements are significantly stronger than breathing motions, and both of them can be easily captured and quantified by it.

Specifically, we define *motion ratio* as the percentage of time when the motion statistic, $\hat{\rho}_b(1/F_s)$, is larger than a preset threshold. Thus for the wake state, a higher motion ratio is expected, as shown in Fig. 12(a). Similarly, we also define *breathing ratio* as the percentage of time when the breathing signal is detected. Since bodily movements destroy the periodicity of the environmental dynamics, the breathing ratio will be lower when a subject is awake, as shown in Fig. 12(b).

2. Note that AASM [40] defines the length of an epoch as 30 seconds, which is based on a high-resolution EEG data. However, for respiratory data, it is recommended to use 300-second epochs to score respiratory events [40], [41]. This is because the average breathing cycle is about 4 seconds, and a 30-second epoch only contains about 7 complete breathing cycles, which are too few to get reliable statistics.

3. Since the respiratory features are only correlated with REM and NREM sleep according to clinical facts [42], respiration-based approaches, including SMARS, could not further differentiate between NREM 1, 2, and 3.

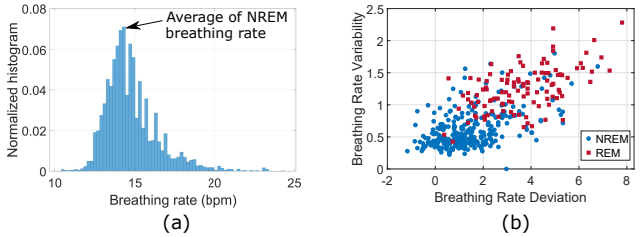

Fig. 13: Features for REM-NREM classification. (a) The histogram of the breathing estimates of a whole night; (b) the distributions of breathing rate deviation and variability for NREM and REM sleep (each dot represents for an epoch).

Combining the above two features, SMARS labels an epoch as sleep only when the motion ratio is smaller than the predefined threshold and the breathing ratio is larger than another threshold. Both thresholds are empirically determined as in Fig. 12. Since our model statistically considers all multipaths indoors, the values of both thresholds generalize to different environments and subjects.

REM/NREM Recognition. SMARS exploits the following clinical facts [42] and accordingly extracts two distinctive features from breathing rate estimates for REM/NREM stages classification: Breathing rate is usually faster and exhibits higher variability and irregular patterns for REM stage, while it is more stable and slower for NREM stage.

Since NREM stage constitutes the majority (about 75% to 80%) of total sleep for typical healthy adults (Fig. 1) [42], the average breathing rate during NREM stage can be estimated by localizing the peak of the histogram of overnight breathing rate estimates, as shown in Fig. 13(a). On this basis, we define *breathing rate deviation*, the distance between the estimated average NREM breathing rate and the 90%-tile of the breathing rate for each epoch, to quantify the deviation of the breathing rate from the baseline during NREM stage.

To extract the variability of the breathing rate for each epoch, we first estimate the trend of breathing rate by applying a 10-th order low-pass Butterworth filter with a normalized cutoff frequency of 0.1 to the breathing estimates of the whole night, and obtain the detrended breathing rate estimates by subtracting the trend from the original breathing rate estimates. Then, the *breathing rate variability* is defined and calculated for each epoch as the variance of the detrended estimates normalized by the length of epoch.

Fig. 13(b) visualizes the distribution of the proposed two features under NREM and REM sleep, respectively. As seen, the majority of the *breathing rate variability* and *breathing rate deviation* of NREM sleep are much smaller than those of REM sleep. Based on these two features, we train a support vector machine (SVM) [43], a widely used binary classifier, to differentiate between REM and NREM sleep.

To be more specific, the radial basis function (RBF) kernel is used in the SVM classifier since the boundary of the two clusters appears to be nonlinear. K-fold cross validation is applied to train the SVM model. The 5 night data with PSG groundtruth has been shuffled randomly and divided into 5 folds. The performance metric of the trained model is obtained by the average of the values computed in each training. Since the typical proportion of REM sleep is only about 20% of the total sleep time, the cost of misclassification for the two classes are also adjusted according to their proportion of appearance, that is, the cost of misclassifying REM as NREM is four times larger than that of misclassifying NREM as REM. Fig. 1 and Fig. 14 show the comparisons between SMARS and the PSG on sleep staging for three nights. Note that the length of each epoch is 300 seconds, and the label of each epoch for both methods represents the majority of the sleep stages within that epoch.

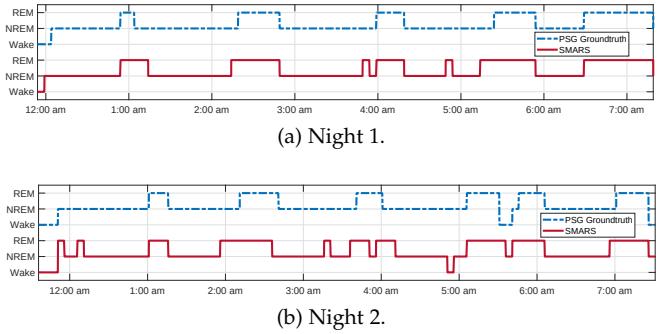

(a) Night 1.

(b) Night 2.

Fig. 14: Comparison between PSG and SMARS on sleep staging in real-world deployment.

4.2.2 *Sleep Quality Assessment*

When we obtain the estimates of wake, REM, and NREM stages of an overnight sleep, we can assess the elusive sleep quality for a user by following standard approach used in clinical practice. In particular, we calculate the sleep score for each night based on the recognized sleep stages as follows. Let T_N, T_R and T_W denote the durations (measured in hours) of NREM sleep, REM sleep and wake, respectively. Since there is no standard formula for sleep score calculation, a simple formula for the sleep score is applied in SMARS [44] [45]:

$$S = 10 * T_N + 20 * T_R - 10 * T_W, \tag{18}$$

which means that longer sleep time and REM duration, less awake time will result in better sleep score. According to recent research [46], REM sleep is crucial for mental recovery, and thus a higher weight has been assigned to REM sleep.

SMARS envisions a practical sleep monitoring for daily in-home use. Although it does not make much sense to compare the sleep score among different users, the trend or history of the sleep score for a particular user would reflect the changes of his/her sleep quality. We believe such results provide clinically meaningful evidences to help diagnose sleep disorders and manage personal health, in an attractive way.

5 Implementation and Evaluation

In this section, we present the system implementation and experimental evaluation of SMARS. We first conduct field studies to evaluate the performance of SMARS and compare it with medical PSG devices as well as other commercial solutions. We then present overnight case studies in 6 homes to show SMARS's capability of monitoring and staging sleep in real-world scenarios.

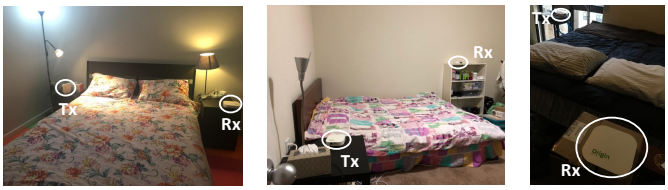

Fig. 15: Experiment settings for sleep monitoring.

5.1 Implementation

We implement a comprehensive system on compact embedded devices for rapid real-world deployment. The devices run Linux with the 3.18.71 kernel and are equipped with commodity Atheros WiFi chipsets. We modify the driver to expose CSI, which is reported with 114 subcarriers for channels on 5.8 GHz WiFi band. Our system consists of a Tx that by default transmits standard WiFi packets at a rate of 30 Hz and an Rx that captures CSI of every packet it received from the Tx. Unless specified otherwise, the Tx is equipped with 2 antennas and the Rx has 3 antennas.

We implement our system in C++, which runs in realtime on the Rx device, calculating the breathing rates and motion statistics as a function of time and sending the data back to a central server via Internet for visualization and sleep staging. The code generates new estimates of both motion and breathing every 1 second. To comprehensively evaluate the impact of different values of the parameters on the performance of SMARS, we also implement a separate realtime version of Matlab code, in the same logic as the C++ code, which runs on a Windows laptop.

5.2 Methodology

Data Collection. Our data collection involves two parts: First, we carry out extensive real-world case studies by deploying our system in 6 homes (including typical houses and apartments) with 6 willing participants. We have 1 female participant and 5 males, aging from 12 to 31 and weighted between 115 and 195 lbs. In total, we collect 32 nights (a total of about 234 hours) of sleep data. Two of the users contributed more than a week's data. Despite the large coverage of SMARS, it is still highly recommended that both of the Tx and Rx are placed close to the bed. This is to make sure that the weak breathing signal can be picked up continuously throughout the whole sleep regardless of different sleep postures and the kinds of quilts used by the user. In addition, especially for the apartment environment, the motion from the neighbors next door would be more unlikely to be detected by SMARS if both the Tx and Rx are placed in the same room. Examples of settings of our devices are shown in Fig. 15, which will be changed by users from one night to another and from one home to another. The receiver is put close to the bed, while the transmitter is placed within the same room for four settings and outside the bedroom for the other two settings. For every night, the users turn on the system for monitoring when they go to bed and stop it after they get up. During sleep, the subjects wear their daily nightgowns and tuck in typical covers like blankets and quilts as they usually do. In addition, the subjects sleep in a natural way, meaning that they are not instructed to lie in a certain position for a certain time period. Instead, they could move their bodies and change sleep postures at will. Normal environmental changes occur regarding the bedroom settings including bedding, tables, closets, *etc.*, during long-term data collection. We note that our study is conducted in real-world scenarios without making any impractical assumptions, completely different from the controlled and short experiments by previous works [5], [11], [12], [13], [14], [15], [27]. All human subjects involved in the data collection were approved by our internal review board (IRB).

Second, we conduct experiments in our lab, a typical office building, to study the coverage of SMARS's motion and breathing detection and further look into the factors which impact the performance. The building contains 10 rooms separated by standard dry walls and furnished with desks, chairs, couches, shelves and computers. During the experiments, there are normal wireless traffics in the air.

To obtain groundtruth labels of sleep stages, we resort to the medical gold standard PSG devices [47]. Participants willing to collect PSG data are dressed with a number of contact sensors that record breathing and sleeping data. During sleep, these sensors and our system are simultaneously recording measurements. In total, we have five nights of PSG data. The PSG data (mainly EEG) are annotated with different sleep stages, according to the AASM specification [40], with an epoch length of 30 seconds. Then every ten of the 30-second epochs are combined to form a 300-second epoch according to the majority voting scheme, which are for the following comparison with SMARS. Breathing rate is derived by the nasal airflow sensor of PSG.

Open dataset. We also validate our system on a public open dataset (denoted as POD in the following) [48], which was recently released by a real-world comparative study [24] on four state-of-the-art RF-based respiratory monitoring systems. The dataset contains 160 hours of overnight sleep data measured from twenty patients, including 11 male participants and 9 females with respective median ages of 55 and 60 years old. The CSI is measured from a 2×2 MIMO system at a sampling rate of 9.9 Hz, with 114 subcarriers on each antenna pair. The PSG data are clinically labeled with detailed sleep stages. In this dataset, all four RF testbeds are positioned in an optimal way so that the link line between Tx and Rx is perpendicular to and on top of the subject's chest. Further details about the dataset can be found in [24], [48].

Comparison. As our system outperforms the state-of-the-art RF-based sleep monitoring works in terms of accuracy, coverage and robustness to diverse working conditions, we choose to compare with commercial products using radar and contact sensors. Specifically, we select ResMed, which employs low-power radar technology, and EMFIT [44], which embeds an array of EMFi sensors into a mat that underpins the mattress. The list prices of ResMed (Sleepscore Max) and EMFIT are $149 and $299, respectively. For comparison, we monitor the participant's sleep with multiple systems simultaneously and compare the overnight outputs of individual technologies. ResMed only works in a short range of up to 2 meters. Thus we place it 1 meter away from the subject's chest during our experiments. As ResMed only provides stage data but no raw breathing data, we only compare sleep staging performance with it.

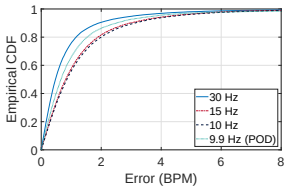

Fig. 16: Overall accuracy of breathing estimation.

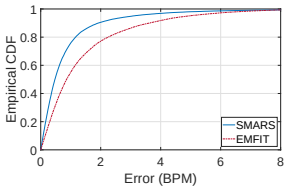

Fig. 17: Accuracy comparison with EMFIT.

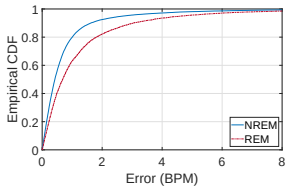

Fig. 18: Breathing estimation for NREM/REM stage.

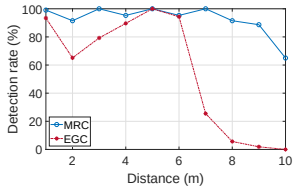

Fig. 19: The impact of MRC on the sensing coverage.

As for the open dataset, we compare the performance of SMARS with the results reported in [24].

5.3 Breathing Estimation Performance

5.3.1 Overall Performance

We study and compare the overall performance of SMARS with the state-of-the-art works and commercial products.

Accuracy. We evaluate the accuracy of breathing rate estimation on both our own measurements and the open dataset. As shown in Fig. 16, evaluation based on our own data demonstrates that SMARS achieves a remarkably high accuracy. In particular, the median error is 0.47 BPM and the 95%-tile error is only 2.92 BPM, using a sampling rate of 30 Hz. Fig. 16 also shows the results based on the open dataset, which demonstrates similar performance with a median error of 0.66 BPM and 95%-tile error of 3.79 BPM. The accuracy is slightly worse since a lower sampling rate of 9.9 Hz is used in the open dataset. As comparison, the real-world study in [24] reported that the best existing system still produces a considerable median error of 2∼3 BPM and a 95%-tile error of about 10 BPM under the same settings.

Besides exceeding existing research proposals, our solution also produces considerably better performance than commercial products based on contact sensors. Specifically, as shown in Fig. 17, SMARS outperforms EMFIT by 0.39 BPM in median error and 1.86 BPM in 95%-tile error. The result is somewhat counter-intuitive since contact sensors should be better in principle. The sensor array of EMFIT, however, is vulnerable to sleeping position and posture, leading to occasionally unreliable estimates during sleep. In contrast, as detailed subsequently, SMARS is more robust regarding sleep position.

Instantaneity. Past works on breathing estimation cannot capture instantaneous respiratory rate changes. A person's breathing rate, however, could change dramatically, especially during REM stage (as measured by PSG in Fig. 1). Thus it is interesting to understand SMARS' capability of tracking instantaneously varying breathing rate, which is critical to sleep staging. For this purpose, we compare the respective estimation accuracy in REM stage that usually observes fast changing breathing and NREM stage that normally observes relatively stable breathing. As illustrated in Fig. 18, SMARS maintains consistently high accuracy, regardless of stable or varying breathing. Although the estimation errors slightly increase with fast changing breathing (during REM stage), the median error is under 0.7 BPM and, more importantly, the changing trend is precisely captured (See upper right of Fig. 1). SMARS outputs one estimate per second in realtime. The main computational complexity of SMARS comes from the estimation of the ACF, giving rise to a computational complexity of $O(|\mathcal{F}|N^2)$, where $|\mathcal{F}|$ denotes the number of available subcarriers and N denotes the number of samples. It takes 0.14 s to process one-second data on a laptop with Intel Core i7 processor and 16 GB memory (Matlab version).

Coverage. SMARS enlarges the sensing coverage to an unparalleled level thanks to its MRC scheme. To quantitatively understand the effective coverage, we conduct experiments in a typical office building. We put a Tx and a Rx, separate by 8.0 meters, and monitor a subject's breathing when he sits at locations that are from 1 to 10 meters away to the link line. We use *detection rate*, defined as the percentage of time when the breathing rate is successfully picked up to the total amount of sleep time, to evaluate the coverage. As shown in Fig. 19, SMARS achieves a detection rate above 90% when the subject is 8 meters away and still retains 88.7% and 65% at distances of 9 meters and 10 meters, respectively. Note that for distances larger than 6 meters, the subject is in another room and has no LOS view to the Tx-Rx link. The coverage is even better than systems using FMCW radar that covers 8 meters [6], not to mention previous WiFi-based approaches that only work when the Tx and Rx are both positioned next to a person with the formed link line fairly close to the person's chest. Although the coverage would be slightly different under different settings (*e.g.*, device placement), our measurements already demonstrate extraordinary coverage that is more than sufficient for practical applications.

Robustness. With the goal of staging sleep, it is critical to continuously monitor breathing throughout the whole night. As verified by [24], however, previous works have frequent periods when breathing cannot be reliably detected. Thus in addition to the accuracy, we would like to understand how robust SMARS is to natural overnight sleep, during which the subject would change postures and move body. As shown in Fig. 22, SMARS consistently reliably detects breathing for 6 different subjects at 6 homes that differ not only in device settings but also in building structure, layout, bedding, and furniture, *etc*. In particular, even in NLOS condition for user 5 and 6 who place the Tx inside the closed closet and outside the bedroom respectively, SMARS yields more than 80% detection rates. Furthermore, Fig. 23 depicts that breathing detection rate for two users' one week data, which demonstrates robustly high detection rate over different nights of natural sleeping. These results suggest that our model is independent of environments and subjects, and is capable of adapting to various scenarios.

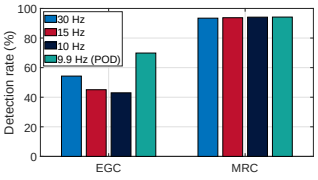

Fig. 20: The impact of different sampling rates.

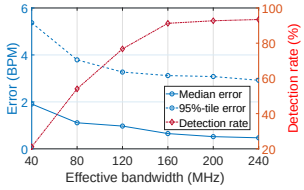

Fig. 21: The impact of effective bandwidth.

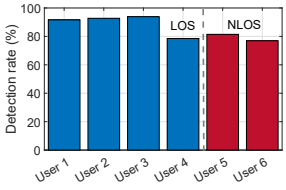

Fig. 22: The breathing detection ratio for six users.

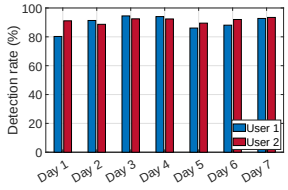

Fig. 23: One week monitoring for 2 users.

5.3.2 Parameter Study

In the following, we examine the key factors that impact the performance of SMARS' breathing estimation.

Impact of MRC. MRC is a key module that improves the accuracy, coverage, and robustness of SMARS. We examine the benefits of MRC by comparing with an equal gain combining (EGC) policy, which basically averages over all subcarriers. As depicted in Fig. 19, MRC remarkably boosts the detection rate in NLOS scenarios (cases with distances >7 meters in Fig. 19) by more than 65% compared to EGC. Fig. 20 further demonstrates significant gains brought by MRC on overnight data. By using MRC, SMARS consistently maintains high detection rates of >90%, regardless of sampling rates of 30 Hz, 20 Hz, or 10 Hz. By comparison, the detection rate of EGC is less than 70% when sampling rate is 30 Hz. While MRC largely improves the detection rate and thus extends the coverage and facilitates the robustness, it provides marginal improvement in accuracy. Specifically, the median accuracy is improved by 0.1 BPM with MRC compared to EGC. The reason is that, as long as breathing can be detected, our ACF-based approach will yield accurate estimate.

Impact of Sampling Rate. We study the impacts of sampling rate on SMARS. As shown in Fig. 16, the median accuracy of breathing estimation decreases from 0.47 BPM to 0.85 BPM when the sampling rate decreases from 30 Hz to 10 Hz. The detection rate, as shown in Fig. 20, does not change too much with respect to sampling rate. Note that both the accuracy and detection rate on the open dataset with 9.9 Hz sampling rate are better than our self-collected data. This is because the open dataset was collected in an optimal setting for previous works, *i.e.*, the Tx and Rx were placed exceedingly close to each other and to the subject, while we deploy the devices in a natural and comfortable manner during our data collection. To conclude, a higher sampling rate will yield better performance while 30 Hz or even 10 Hz is adequate in practice.

Impact of Effective Bandwidth. We study the impacts of frequency diversity attributed by antennas via effective bandwidth defined as $W_e \triangleq N_s B$, where N_s denotes the number of spatial streams between the Tx and Rx, and B denotes the bandwidth of each stream (40 MHz in our system). Fig. 21 shows that with the increasing of effective bandwidth, the median error and 95%-tile error decrease, and at the same time, the detection rate increases. The results suggest that a 2×2 MIMO system (*i.e.*, 160 MHz effective bandwidth) is sufficient for SMARS to achieve a remarkable performance.

TABLE 1: Comparison of different sleep monitoring systems.

	Overall	Wake	Sleep	REM	NREM
SMARS	88.4%	86.7%	96.3%	86.9%	89.1%
EMFIT	69.8%	76.7%	98.2%	46.3%	74.9%
ResMed	81.2%	52.6%	95.3%	78.9%	87.2%

5.4 Sleep Staging Performance

In this section, we evaluate the performance in sleep staging and compare with commercial products. We further carry out a two-week case study for long-term daily sleep monitoring.

5.4.1 Sleep Stage Recognition Accuracy

We summarize the accuracy of SMARS compared to two commercial products EMFIT and ResMed in Table 1. Fig. 24 shows the more detailed confusion matrices. As can be seen, SMARS yields an overall accuracy of 88.4% in sleep staging, outperforming commercial solutions EMFIT and ResMed, which use contact sensors and UWB radar respectively. In particular, SMARS achieves a recognition accuracy of 87%, 89% and 87% for wake/NREM/REM detection respectively, which is better than EMFIT and ResMed. Note that EMFIT performs staging with additional heart rate measurements, ResMed further incorporates microphones (from their smartphone APP), while SMARS purely relies on breathing and motion estimation.

Regarding the public open dataset, SMARS cannot perform sleep staging well for those patients, although remarkable accuracy in breathing estimation is achieved. This is because, for those patients with severe diseases, such as sleep apnea and periodic limb movement syndrome (PLMS), their breathing pattern is not only affected by sleep stages but also by the inherent, erratic chest movement and abnormal respiration caused by the diseases [49]. Fig. 25 illustrates the overnight breathing, both the ground truths and our estimates, for an elderly patient. As seen, the breathing patterns fluctuate and do not exhibit distinguishable patterns we observed in healthy subjects as in Fig. 1. As a consequence, the natural relationship between breathing patterns and sleep stages no longer holds for this patient. In the future, we intend to study SMARS on a broad spectrum of patients, ranging from normal subjects to those with chronic sleep disorders. From these studies, we hope to unveil the capabilities of SMARS as a diagnostic instrument, and also as a supplementary health monitoring technology.

5.4.2 Long-term Daily Assessment of Sleep

To demonstrate the capability of SMARS for daily sleep monitoring, we carry out a two-week case study for a specific user. Every night, the participant sleeps with our

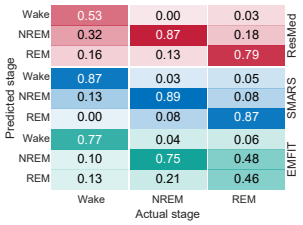

Fig. 24: Confusion matrix of ResMed, SMARS, and EMFIT.

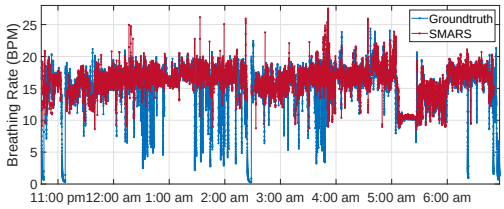

Fig. 25: The breathing monitoring result for a typical patient in the open dataset.

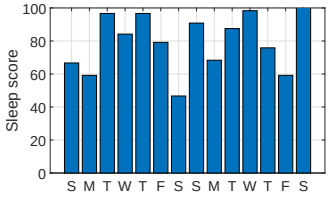

Fig. 26: Sleep quality assessment over two weeks.

system running. During the data collection, the bedroom environments, device locations, in addition to the bedding and his nightclothes will change from night to night. Here we assess the user's sleep quality by calculating the sleep score as specified in (18). Fig. 26 illustrates the historical scores over the two-week term. Based on these quantitative sleep quality statistics, SMARS offers useful data for personal healthcare.

6 Conclusion

This paper presents the design, implementation, and evaluation of SMARS, the first practical sleep monitoring system that exploits ambient radio signals to recognize sleep stages, without instrumenting users' body or the bed. SMARS achieves this goal by monitoring breathing and body movements during sleep accurately and instantaneously, to a level of performance previously only attainable with expensive specialized infrastructure. A key enabler behind is a statistical model that considers all reflection and scattering multipaths indoors without making unrealistic assumptions. We implement SMARS on commercial WiFi chipsets and validate its performance on single-person sleep monitoring by extensive experiments with 32 nights of data collected in 6 homes. We believe SMARS takes a promising step towards practical in-home sleep monitoring.

References

[1] N. I. of Health, "Brain basics: Understanding sleep." http://www.ninds.nih.gov/disorders/brain_basics/understanding_sleep.htm#sleep_disorders, 2018.

[2] Centers for Disease Control and Prevention, "Short sleep duration among us adults." https://www.cdc.gov/sleep/data_statistics.html, 2018.

[3] G. Matar, J.-M. Lina, J. Carrier, and G. Kaddoum, "Unobtrusive sleep monitoring using cardiac, breathing and movements activities: an exhaustive review," *IEEE Access*, vol. 6, pp. 45129–45152, 2018.

[4] T. Penzel, N. Wessel, M. Riedl, J. W. Kantelhardt, S. Rostig, M. Glos, A. Suhrbier, H. Malberg, and I. Fietze, "Cardiovascular and respiratory dynamics during normal and pathological sleep," *Chaos: An Interdisciplinary Journal of Nonlinear Science*, vol. 17, no. 1, p. 015116, 2007.

[5] C. Wu, Z. Yang, Z. Zhou, X. Liu, Y. Liu, and J. Cao, "Non-invasive detection of moving and stationary human with wifi," *IEEE Journal on Selected Areas in Communications*, vol. 33, pp. 2329–2342, Nov 2015.

[6] F. Adib, H. Mao, Z. Kabelac, D. Katabi, and R. C. Miller, "Smart homes that monitor breathing and heart rate," in *Proceedings of the 33rd Annual ACM Conference on Human Factors in Computing Systems (CHI)*, 2015.

[7] W. Wang, A. X. Liu, M. Shahzad, K. Ling, and S. Lu, "Understanding and modeling of wifi signal based human activity recognition," in *Proceedings of the 21st Annual International Conference on Mobile Computing and Networking (MobiCom)*, 2015.

[8] K. Qian, C. Wu, Z. Yang, Y. Liu, and Z. Zhou, "Pads: Passive detection of moving targets with dynamic speed using phy layer information," in *IEEE International Conference on Parallel and Distributed Systems*, December 16 - 19 2014.

[9] C.-Y. Hsu, A. Ahuja, S. Yue, R. Hristov, Z. Kabelac, and D. Katabi, "Zero-effort in-home sleep and insomnia monitoring using radio signals," *Proceedings of the ACM on Interactive, Mobile, Wearable and Ubiquitous Technologies (UbiComp)*, vol. 1, pp. 59:1–59:18, Sept. 2017.

[10] M. Zhao, S. Yue, D. Katabi, T. S. Jaakkola, and M. T. Bianchi, "Learning sleep stages from radio signals: A conditional adversarial architecture," in *Proceedings of the 34th International Conference on Machine Learning (ICML)*, vol. 70, 06–11 Aug 2017.

[11] X. Liu, J. Cao, S. Tang, and J. Wen, "Wi-sleep: Contactless sleep monitoring via wifi signals," in *Proceedings of the IEEE Real-Time Systems Symposium (RTSS)*, Dec 2014.

[12] J. Liu, Y. Wang, Y. Chen, J. Yang, X. Chen, and J. Cheng, "Tracking vital signs during sleep leveraging off-the-shelf wifi," in *Proceedings of the 16th ACM International Symposium on Mobile Ad Hoc Networking and Computing (MobiHoc)*, 2015.

[13] X. Wang, C. Yang, and S. Mao, "Tensorbeat: Tensor decomposition for monitoring multiperson breathing beats with commodity wifi," *ACM Transactions on Intelligent Systems and Technology*, vol. 9, pp. 8:1–8:27, Sept. 2017.

[14] H. Wang, D. Zhang, J. Ma, Y. Wang, Y. Wang, D. Wu, T. Gu, and B. Xie, "Human respiration detection with commodity wifi devices: Do user location and body orientation matter?," in *Proceedings of the ACM International Joint Conference on Pervasive and Ubiquitous Computing (UbiComp)*, 2016.

[15] F. Zhang, D. Zhang, J. Xiong, H. Wang, K. Niu, B. Jin, and Y. Wang, "From fresnel diffraction model to fine-grained human respiration sensing with commodity wi-fi devices," *Proceedings of the ACM on Interactive, Mobile, Wearable and Ubiquitous Technologies (UbiComp)*, vol. 2, pp. 53:1–53:23, Mar. 2018.

[16] J. S. Seybold, *Introduction to RF propagation*. John Wiley & Sons, 2005.

[17] W. M. Gifford, W. W. L. Li, Y. J. Zhang, and M. Z. Win, "Effect of bandwidth on the number of multipath components in realistic wireless indoor channels," in *Proceedings of the IEEE International Conference on Communications (ICC)*, June 2011.

[18] P. Nguyen, X. Zhang, A. Halbower, and T. Vu, "Continuous and fine-grained breathing volume monitoring from afar using wireless signals," in *Proceedings of the 35th Annual IEEE International Conference on Computer Communications (INFOCOM)*, 2016.

[19] J. Yang, J. M. Keller, M. Popescu, and M. Skubic, "Sleep stage recognition using respiration signal," in *Proceedings of the 38th Annual International Conference of the Engineering in Medicine and Biology Society (EMBC)*, 2016.

[20] A. Nguyen, R. Alqurashi, Z. Raghebi, F. Banaei-Kashani, A. C. Halbower, and T. Vu, "A lightweight and inexpensive in-ear sensing system for automatic whole-night sleep stage monitoring," in *Proceedings of the 14th ACM Conference on Embedded Network Sensor Systems (SenSys)*, 2016.

[21] T. Hao, G. Xing, and G. Zhou, "isleep: unobtrusive sleep quality monitoring using smartphones," in *Proceedings of the 11th ACM Conference on Embedded Networked Sensor Systems (SenSys)*, 2013.

[22] J.-K. Min, A. Doryab, J. Wiese, S. Amini, J. Zimmerman, and J. I. Hong, "Toss'n'turn: smartphone as sleep and sleep quality detector," in *Proceedings of the SIGCHI conference on human factors in computing systems (CHI)*, 2014.

[23] Z. Chen, M. Lin, F. Chen, N. D. Lane, G. Cardone, R. Wang, T. Li, Y. Chen, T. Choudhury, and A. T. Campbell, "Unobtrusive sleep monitoring using smartphones," in *Proceedings of the 7th International Conference on Pervasive Computing Technologies for Healthcare*, 2013.

[24] P. Hillyard, A. Luong, A. S. Abrar, N. Patwari, K. Sundar, R. Farney, J. Burch, C. A. Porucznik, and S. Pollard, "Experience: Cross-technology radio respiratory monitoring performance study," in *Proceedings of the 24th Annual International Conference on Mobile Computing and Networking (MobiCom)*, Oct 2018.

[25] F. Lin, Y. Zhuang, C. Song, A. Wang, Y. Li, C. Gu, C. Li, and W. Xu, "Sleepsense: A non-contact and cost-effective sleep monitoring system," *IEEE Transactions on Biomedical Circuits and Systems*, vol. 11, pp. 189–202, Feb 2017.

[26] T. Rahman, A. T. Adams, R. V. Ravichandran, M. Zhang, S. N. Patel, J. A. Kientz, and T. Choudhury, "Dopplesleep: A contactless unobtrusive sleep sensing system using short-range doppler radar," in *Proceedings of the 2015 ACM International Joint Conference on Pervasive and Ubiquitous Computing (UbiComp)*, (New York, NY, USA), 2015.

[27] Z. Yang, P. H. Pathak, Y. Zeng, X. Liran, and P. Mohapatra, "Vital sign and sleep monitoring using millimeter wave," *ACM Transactions on Senor Networks*, vol. 13, pp. 14:1–14:32, Apr. 2017.

[28] O. J. Kaltiokallio, H. Yigitler, R. Jäntti, and N. Patwari, "Non-invasive respiration rate monitoring using a single cots tx-rx pair," in *Proceedings of the 13th international symposium on information processing in sensor networks (IPSN)*, 2014.

[29] N. Patwari, L. Brewer, Q. Tate, O. Kaltiokallio, and M. Bocca, "Breathfinding: A wireless network that monitors and locates breathing in a home.," *IEEE Journal of Selected Topics in Signal Processing*, vol. 8, no. 1, pp. 30–42, 2014.

[30] K. Ali, A. X. Liu, W. Wang, and M. Shahzad, "Keystroke recognition using wifi signals," in *Proceedings of the 21st Annual International Conference on Mobile Computing and Networking (MobiCom)*, 2015.

[31] J. Zhang, Z. Tang, M. Li, D. Fang, P. T. Nurmi, and Z. Wang, "Crosssense: towards cross-site and large-scale wifi sensing," 2018.

[32] W. Jiang, C. Miao, F. Ma, S. Yao, Y. Wang, Y. Yuan, H. Xue, C. Song, X. Ma, D. Koutsonikolas, *et al.*, "Towards environment independent device free human activity recognition," 2018.

[33] D. Tse and P. Viswanath, *Fundamentals of wireless communication*. Cambridge university press, 2005.

[34] H. Kaneko and J. Horie, "Breathing movements of the chest and abdominal wall in healthy subjects," *Respiratory care*, vol. 57, no. 9, pp. 1442–1451, 2012.

[35] F. Zhang, C. Chen, B. Wang, and K. R. Liu, "Wispeed: A statistical electromagnetic approach for device-free indoor speed estimation," *IEEE Internet of Things Journal*, vol. 5, no. 3, pp. 2163–2177, 2018.

[36] R. H. Shumway and D. S. Stoffer, "Time series analysis and its applications with r examples," *Time series analysis and its applications with R examples*, 2006.

[37] W. S. Cleveland, "Robust locally weighted regression and smoothing scatterplots," *Journal of the American statistical association*, vol. 74, no. 368, pp. 829–836, 1979.

[38] J. R. Barry, E. A. Lee, and D. G. Messerschmitt, *Digital communication*. Springer Science & Business Media, 2012.

[39] C. Chen, Y. Han, Y. Chen, H.-Q. Lai, F. Zhang, B. Wang, and K. R. Liu, "Tr-breath: Time-reversal breathing rate estimation and detection," *IEEE Transactions on Biomedical Engineering*, vol. 65, no. 3, pp. 489–501, 2018.

[40] "The aasm manual for the scoring of sleep and associated events." https://aasm.org/clinical-resources/scoring-manual/. Accessed: 2019-05-31.

[41] C. W. Whitney, D. J. Gottlieb, S. Redline, R. G. Norman, R. R. Dodge, E. Shahar, S. Surovec, and F. J. Nieto, "Reliability of scoring respiratory disturbance indices and sleep staging," *Sleep*, vol. 21, no. 7, pp. 749–757, 1998.

[42] B. M. Altevogt, H. R. Colten, *et al.*, *Sleep disorders and sleep deprivation: an unmet public health problem*. National Academies Press, 2006.

[43] C. J. Burges, "A tutorial on support vector machines for pattern recognition," *Data mining and knowledge discovery*, vol. 2, no. 2, pp. 121–167, 1998.

[44] "Emfit sleep tracking & monitoring with heart-rate-variability." https://www.emfit.com/, 2018.

[45] J. M. Kortelainen, M. O. Mendez, A. M. Bianchi, M. Matteucci, and S. Cerutti, "Sleep staging based on signals acquired through bed sensor," *IEEE Transactions on Information Technology in Biomedicine*, vol. 14, no. 3, pp. 776–785, 2010.

[46] I. Lerner, S. M. Lupkin, N. Sinha, A. Tsai, and M. A. Gluck, "Baseline levels of rapid eye movement sleep may protect against excessive activity in fear-related neural circuitry," *Journal of Neuroscience*, vol. 37, no. 46, pp. 11233–11244, 2017.

[47] "Alice pdx: portable sleep diagnostic system." https://www.philips.com.hk/healthcare/product/HC1043941/alice-pdx-portable-sleep-diagnostic-system, note = Accessed: 2019-01-06.

[48] P. Hillyard, "Rf respiration monitoring dataverse." https://doi.org/10.7910/DVN/X7AYXQ, 2018.

[49] W. Bara-Jimenez, M. Aksu, B. Graham, S. Sato, and M. Hallett, "Periodic limb movements in sleep: state-dependent excitability of the spinal flexor reflex," *Neurology*, vol. 54, no. 8, pp. 1609–1616, 2000.

Feng Zhang (S'12) received his B.S. and M.S. degrees from the Department of Electronic Engineering and Information Science, University of Science and Technology of China, Hefei, in 2011 and 2014, respectively. He received his Ph.D. degree from the Department of Electrical and Computer Engineering, University of Maryland, College Park in 2018. He is currently with Origin Wireless, Inc. His research interests include wireless sensing, statistical signal processing, and wireless indoor localization. He was the recipient of Distinguished TA award from the University of Maryland and the State Scholarship from the University of Science and Technology of China.

Chenshu Wu (M'15) received his B.E. degree in School of Software in 2010 and Ph.D. degree in Department of Computer Science in 2015, both from Tsinghua University, Beijing, China. He is now a Postdoc Research Associate in the Department of Electrical & Computer Engineering University of Maryland, College Park and a Principal Scientist at Origin Wireless Inc. His research interests include Internet of Things and mobile computing. He is a member of the IEEE and the ACM.

Beibei Wang (SM'15) received the B.S. degree in electrical engineering (with the highest honor) from the University of Science and Technology of China, Hefei, in 2004, and the Ph.D. degree in electrical engineering from the University of Maryland, College Park in 2009. She was with the University of Maryland as a research associate in 2009-2010, and with Qualcomm Research and Development in 2010-2014. Since 2015, she has been with Origin Wireless Inc. where she is now a chief scientist. Her research interests include wireless communications and signal processing. Dr. Wang received the Graduate School Fellowship, the Future Faculty Fellowship, and the Dean's Doctoral Research Award from the University of Maryland, and the Overview Paper Award from IEEE Signal Processing Society in 2015. She is a co-author of Cognitive Radio Networking and Security: A Game-Theoretic View (Cambridge University Press, 2010).

Min Wu (S'95-M'01-SM'06-F'11) received the B.E. degree in electrical engineering and the B.A. degree in economics from Tsinghua University, Beijing, China, in 1996 with the Highest Honors, and the Ph.D. degree in electrical engineering from Princeton University in 2001. Since 2001, she has been with the University of Maryland, College Park, where she is currently a Professor and the University Distinguished Scholar-Teacher. She leads the Media and Security Team University of Maryland, with main research interests on information security and forensics and multimedia signal processing.

She was elected as an IEEE Fellow and an AAAS Fellow for contributions to signal processing, multimedia security, and forensics. She was a co-recipient of the two best paper awards from the IEEE Signal Processing Society and EURASIP. She received the NSF CAREER Award in 2002, the TR100 Young Innovator Award from MIT Technology Review Magazine in 2004, the ONR Young Investigator Award in 2005, the ComputerWorld 40 Under 40 IT Innovator Award in 2007, the IEEE Mac Van Valkenburg Early Career Teaching Award in 2009, and the IEEE Distinguished Lecturer recognition for 2015–2016. She has served as the Vice President-Finance of the IEEE Signal Processing Society from 2010 to 2012. She has served as the Chair of the IEEE the Technical Committee on Information Forensics and Security from 2012 to 2013. She has also served as the Editor-in-Chief for the IEEE Signal Processing Magazine from 2015 to 2017.

Daniel Bugos received his B.S. degree in the Department of Computer Science from the University of Maryland, College Park, in 2018. He is now with Origin Wireless Inc. His research interests include IoT healthcare solutions, contact-free vital sign monitoring, and smart home networks.

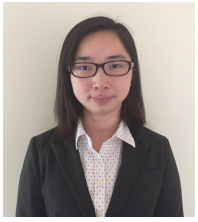

Hangfang Zhang (S'15) is currently an Embedded Architect in Origin Wireless, Inc in Greenbelt, MD. She has received her PhD degree in Electrical Engineering in Vanderbilt University in 2018 and BS degree in Electrical Engineering from University of Science and Technology of China in 2011. Her work focuses on hardware development and system reliability for embedded systems.

K. J. Ray Liu (F'03) was named a Distinguished Scholar-Teacher of University of Maryland, College Park, in 2007, where he is Christine Kim Eminent Professor of Information Technology. He leads the Maryland Signals and Information Group conducting research encompassing broad areas of information and communications technology with recent focus on wireless AI. Dr. Liu is IEEE Vice President, Technical Activities – Elect. He was President of IEEE Signal Processing Society, where he has served as Vice President – Publications and Board of Governor, and a member of IEEE Board of Director as Division IX Director. He has also served as the Editor-in-Chief of IEEE Signal Processing Magazine.

Dr. Liu was a recipient of the 2016 IEEE Leon K. Kirchmayer Award on graduate teaching and mentoring, IEEE Signal Processing Society 2014 Society Award, IEEE Signal Processing Society 2009 Technical Achievement Award, and over a dozen of best paper awards. Recognized by Web of Science as a Highly Cited Researcher, he is a Fellow of IEEE and AAAS. His invention of Time-Reversal Machine by Origin Wireless Inc. won the 2017 CEATEC Grand Prix award.

Dr. Liu is IEEE Vice President, Technical Activities – Elect. He was President of IEEE Signal Processing Society, where he has served as Vice President – Publications and Board of Governor, and a member of IEEE Board of Director as Division IX Director. He has also served as the Editor-in-Chief of IEEE Signal Processing Magazine.

He also received teaching and research recognitions from University of Maryland including university-level Invention of the Year Award; and college-level Poole and Kent Senior Faculty Teaching Award, Outstanding Faculty Research Award, and Outstanding Faculty Service Award, all from A. James Clark School of Engineering.